IEEE Access
Multidisciplinary | Rapid Review | Open Access Journal

Received August 4, 2018, accepted September 10, 2018, date of publication September 20, 2018, date of current version October 17, 2018.

Digital Object Identifier 10.1109/ACCESS.2018.2871123

Image Dehazing Based on Robust Sparse Representation

SHUYING HUANG[1], (Member, IEEE), DONGLEI WU[1], YONG YANG[2], (Senior Member, IEEE), AND HAIJUN ZHU[1]

[1]School of Software and Communication Engineering, Jiangxi University of Finance and Economics, Nanchang 330032, China
[2]School of Information Technology, Jiangxi University of Finance and Economics, Nanchang 330032, China

Corresponding author: Yong Yang (greatyangy@126.com)

This work was supported in part by the National Natural Science Foundation of China under Grant 61662026, Grant 61862030, and Grant 61462031, in part by the Natural Science Foundation of Jiangxi Province under Grant 20181BAB202010, and in part by the Project of the Education Department of Jiangxi Province under Grant GJJ170318, Grant GJJ170312, and Grant KJLD14031.

ABSTRACT One source of difficulties when processing outdoor images is the presence of haze, smoke, or fog, which reduces the contrast and fades the colors of the observed object. To overcome this problem, we propose a novel single-image dehazing method based on robust sparse representation in this paper. First, we propose to employ the robust sparse representation on the color and luminance channels of the hazy image to obtain the haze density information. Then, we introduce the haze density information to estimate the transmission. Using the method based on the atmospheric scattering model, we can directly recover a natural haze-free image. Finally, in order to improve the visual quality of the dehazed image, a post-processing procedure is designed to enhance the visibility. We conduct the experiments on diverse types of hazy images and the experimental results show that the proposed method based on robust sparse representation outperforms several traditional and state-of-the-art methods.

INDEX TERMS Single image dehazing, robust sparse representation, atmospheric scattering model, visibility.

I. INTRODUCTION

The quality of images is important in the fields of computer vision applications, such as object detection, scene analysis and traffic monitoring. However, outdoor images suffer from bad weather conditions that directly cause the deterioration of the image quality. The typical effects that result from haze, mist and smoke greatly decrease the visibility and contrast. According to the research of reference [1], the phenomena of haze, mist and smoke leads to atmospheric absorption and scattering. The radiation of light received by the camera is degraded along the line of the scene. Moreover, the incoming light mixed with global atmospheric light generates a veil that affects the captured image and can be considered as a haze component of the image. As shown in Fig.1(a), haze can tremendously reduce the color fidelity, color contrast and the accuracy of computer vision. Hence, image dehazing technology became a severe challenge in recent years and has essential research significance and value. Fig. 1(b) shows the result of image dehazing on Fig.1(a).

(a) (b)

FIGURE 1. Haze removal for a single image. (a) Input haze image. (b) Dehazing result.

Single image haze removal has been improved rapidly in recent years. Based on various principles of single image dehazing, existing methods can be divided into two categories: image enhancement-based dehazing methods and image restoration model-based dehazing methods.

Image enhancement-based methods do not consider the causes of image degradation, but directly improve the contrast and visibility of the target images. Inspired by the observation that a haze-free image must have higher contrast compared with its hazy version, Tan [2] proposed a typical method based on local contrast maximization. The method can well

handle the regions with heavy haze. However, this algorithm generates color distortion because of the lack of physical information. Tarel and Hautière [3] enhanced the contrast of an image by assuming that the depth map of a foggy image is smooth except for the edge regions. Although this method has achieved an effective computation, it cannot handle the discontinuous scene depth regions well. Recently, many dehazing methods based on image fusion have also been proposed by fusing multiple images into a single image to enhance the useful features. For example, Choi *et al*. [4] proposed a fusion-based method by fusing the haze aware statistical feature to enhance the visibility of a single hazy image. Galdran *et al*. [5] proposed a fusion-based variational image-dehazing algorithm, which enhanced a hazy image by maximizing contrast and saturation on the hazy input. However, the limitation of enhancement-based methods is the absence of physical information, which will lead to over-enhancement or distortion.

Recently, the model-based image dehazing methods have made significant progress. These methods were mainly devoted to estimate the parameters of atmospheric scattering model to remove haze. Chavez [6] proposed a novel contrast enhancement method that subtracts the offset value determined by the distribution of the darkest object intensity. This method is effective for hazy images with homogeneous scenes. Fattal [7] proposed a method for image restoration by assuming that transmission and surface shading are statistically uncorrelated to infer the medium transmission. This method can well remove thin haze from images but fails to remove heavy fog. Meanwhile, it may not work when the statistical hypotheses fail. The well-known method proposed by He *et al*. [8] made an important contribution to haze removal by introducing a statistical observation called the Dark Channel Prior, which states that at least one color channel exists with one low-intensity pixel close to zero for most non-sky patches. With this prior, transmission can be estimated by employing the minimization filter twice. Some improved algorithms [9]–[13] were proposed to refine the rough transmission map and yielded better results. However, the dark channel prior assumption might be invalid when the large bright areas such as sky, water, or white object regions exist in hazy images. Based on a new geometric perspective for dark channel prior theory, Meng *et al*. [14] designed an inherent boundary constraint from the radiance cube to estimate the transmission map by using a morphological closing operator for the bright region. Nishino *et al*. [15] introduced a probabilistic approach based on Bayesian theory for haze removal. This method regarded scene albedo and depth as two statistically independent latent layers and formulated a factorial Markov random field of the hazy image to jointly estimate the transmission and depth information. Wang and Fan [16] proposed a multiscale depth fusion (MDP) scheme using an inhomogeneous Laplacian–Markov random field to obtain the depth information of the physical model. Hautière *et al*. [17] computed the scene information by employing a board optical sensor system to build a geographical model. Later, Kim *et al*. [18] removed haze by building a cost function based on the degree of information loss, which keeps the balance between contrast improvement and information loss. These model-based methods remove haze by analyzing the mechanism of image degradation and have obtained outstanding achievements.

In addition, learning-based dehazing algorithms have been studied recently. Tang *et al*. [19] researched various haze-relevant features to identify the best haze-relevant feature and estimated the transmission with Random Forests. Zhu *et al*. [20] designed a linear model to estimate the depth information based on the color attenuation prior, and used a supervised method to learn the parameters. Despite the significant progress obtained by machine learning methods, these state-of-the-art methods are limited by their manual features. Thanks to the development of deep learning and Convolutional Neural Networks (CNNs), Cai *et al*. [21] proposed a deep-learning network that is an end-to-end system for medium transmission estimation. Recently, Li *et al*. [22] proposed a cascaded CNN to jointly estimate medium transmissions and global atmospheric light under two subnetworks. Obviously, the general difficulty faced by these learning-based methods is hard to obtain a substantial and appropriate training data for training the model. The dehazed result will be strongly affected by this difficulty.

Since the model-based methods possess the advantage of preserving physical information that yields more realistic results, our research is also proceeded in this way. For the model-based image dehazing methods, one of the key points is to estimate the parameters of the atmospheric scattering model. As we know, the haze density is one of the most important features of a hazy image, and it is similar to an ''atmospheric veil'' [3]. Thus, our work is to estimate the parameters of the model by studying the substantive features of the deteriorated images instead of studying the degradation process. According to our research, the ''atmospheric veil'' has a negative correlation with the medium transmission. Therefore, the haze density map in a hazy image is most likely to be a clue for estimating the transmission map. Based on the above analysis, we attempt to establish a contact with the transmission and haze density. As is well-known, the image can be decomposed into low frequency information representing the intensity changes of the whole image and high frequency information r representing the intensity changes of the whole image and high frequency information representing the edges and contours of the image [23]. By observation (e.g., Fig. 2), we can find that there is a certain relationship between the intensity changes of the image and haze density, and thus we attempt to employ low-frequency components to construct the haze density map. Then, the density map is applied to estimate the transmission and atmospheric light. Finally, the clear image can be obtained by inverting the atmospheric scattering model. In this paper, we introduce an improved sparse representation method, called the robust sparse representation (RSR) [24], to extract the intensity changes of the haze image in the luminance space.

FIGURE 2. Image robust sparse representation process. *Y* denotes a hazy image. *D* is a dictionary and *X* is the corresponding sparse representation coefficients. *DX* denotes a low frequency version of the image and error term *E* denotes a high frequency version containing the edge information of the image.

Compared with traditional sparse representation, the RSR improves the robustness to non-Gaussian noise. Both subjective and objective evaluations of the experiments have proved the effectiveness of the proposed method.

The main contributions of this paper are summarized as follows:

1) In this paper, an effective single image dehazing method is proposed based on RSR decomposition and adaptive luminance adjustment. Experiments show that our method can obtain better dehazing images with more details and less color distortions.

2) The RSR method is the first attempt to estimate the transmission map, and it is used to decompose the haze images into the intensity map and the detail map. The intensity map is employed to estimate the transmission map, which takes account into the information of image color and brightness and makes the dehazing results look more natural.

3) To appropriately enhance the visuality of dehazed image, an adaptive luminance transformation function is designed by conducting a nonlinear transformation procedure in the luminance space of the dehazed images. Compared with original dehazed images, the refined dehazed images possess richer details.

The rest of the paper is organized as follows. The background theory is introduced briefly in Section 2. The details of our proposed dehazing algorithm are elaborated in Section 3, including the evaluation of the transmission map and the atmospheric light value, and the adaptive luminance transformation for the raw dehazed image. Then, we give the experimental results in Section 4, in which the dehazed results and the corresponding quantitative assessments compared with the state-of-the-art methods are given. Finally, we summarize our methods in Section 5.

II. GUIDELINES FOR MANUSCRIPT PREPARATION

The atmospheric scattering model is widely used to describe the degradation of hazy and foggy images [1]. The general formulation is given below:

$$\boldsymbol{I}(x) = \boldsymbol{J}(x)t(x) + \boldsymbol{A}(1 - t(x)) \tag{1}$$

where $\boldsymbol{I}$ is the observed hazy image, $\boldsymbol{J}$ is the scene radiance of the haze-free image, $\boldsymbol{A}$ is the atmospheric light, and $\boldsymbol{x}$ is the coordinate of the pixel. $\boldsymbol{t}$ is the medium transmission between the object and the camera, which ranges from 0 to 1.

The target of image dehazing is to recover J from Eq. (1) by estimating A and $t(x)$. Here, the first part $J(x)t(x)$ represents the direct attenuation, and it means that the scene radiance is attenuated by the transmission characteristic of the medium. The second part $A(1\text{-}t(x))$ is called the airlight [1], [3], which leads to the loss of propagation and color shifting. In the condition of a homogeneous medium, the medium transmission t can be expressed as follows:

$$t(x) = e^{-\beta d(x)} \tag{2}$$

where β is the medium attenuation coefficient and d(x) is the distance between the observer and surface of the object. Eq. (2) means that the scenic radiance attenuates exponentially with the scenic depth d.

III. HAZE REMOVAL BY ROBUST SPARSE REPRESENTATION

In this section, the proposed method will be divided into a three-step procedure and a post-processing procedure. The whole framework is illustrated in Fig. 3. In Part 1, we propose a method of designing the dictionary and get the intensity map of the foggy image by RSR decomposition. Then, we employ the intensity map to estimate the transmission map in Part 2. In Part 3, the haze-free image is recovered by inverting the atmospheric scattering model. Finally, adaptive luminance transformation is introduced to adjust the brightness of the dehazing image.

A. RSR DECOMPOSITION

As we know, in different regions of a hazy image, the haze density is different. Visually, in the distant regions with heavy haze, the pixels in the image have higher intensity values. Whereas, in the near regions with thin haze, the pixels in the image have lower intensity values. Hence, the pixel's intensity information reflects the haze density well in a hazy image. From the above analysis, we can infer that the intensity channel of an image contains the abundant luminance information. To estimate the transmission map, the intensity map of the haze image is first obtained by the RSR decomposition. However, color distortions usually occur in image dehazing algorithms, so we proposed a method (shown in Fig. 4) to construct the dictionaries using red, green, blue and luminance components respectively. The specific process is described as follows.

We first slide a small window with a fixed step on each of the four channels to take image blocks. Then, each image block is vectored, and all vectors of each channel are arranged into a vector matrix. Finally, every vector matrix is normalized to obtain the dictionary D of each channel (see from Part 1 in Fig. 3). A large number of experiments demonstrate that 45×45 is the proper window size in this paper. Here, the four channels of the hazy image are decomposed by the RSR, which is expressed as

$$Y_C = D_C X_C + E_C \tag{3}$$

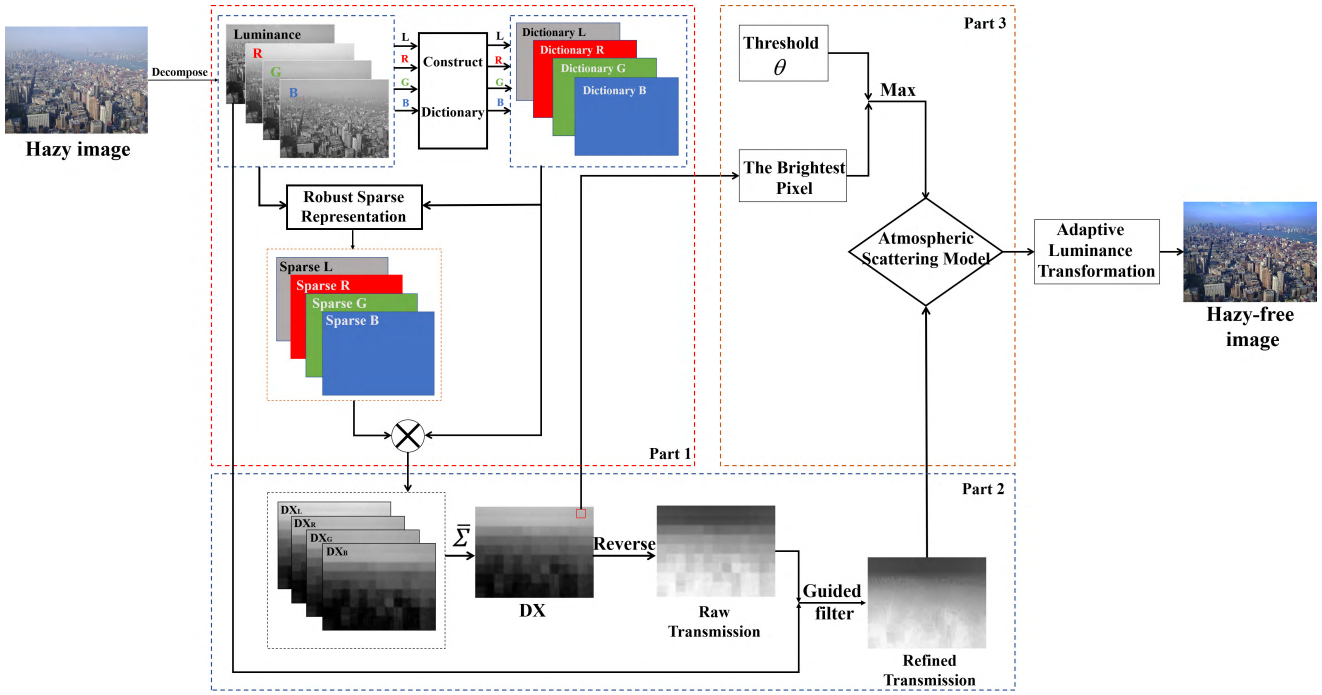

FIGURE 3. The framework of the proposed method.

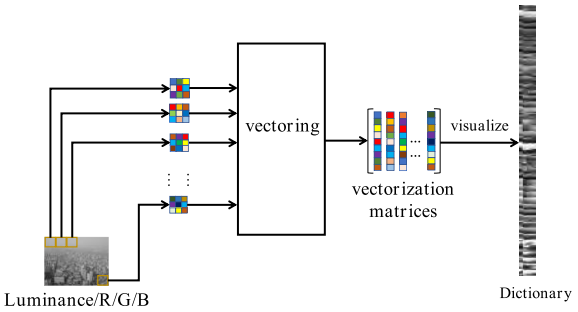

FIGURE 4. The process of constructing the dictionary.

where C represents four channels $\{R, G, B, and\ L\}$, R, G, B, and L represent red, green, blue and luminance respectively. Y is an observed hazy image, D is the dictionary we obtained, and E is the error matrix. X is the matrix of the sparse coefficients in which most elements are zero. DX and E denote the reconstruction matrix (*i.e.* the low-frequency components) and the error matrix (*i.e.* the edge details), respectively. The sparse decomposition of Y can be obtained by solving the following l_0-minimization problem:

$$\min_{X_C, E_C} = \|X_C\|_0 + \lambda \|E_C\|_{2,0} \quad s.t.\ Y_C = D_C X_C + E_C \qquad (4)$$

where $||X_C||_0$denotes its l_0-norm. $||E_C||_{2,\ 0}$ denotes the l_2-norm of the error matrix E_C, which is used to describe sample-specific error terms and outliers [25]. E always contains rich edge information of Y. The parameter $\lambda > 0$ is set to balance the influence of the two components $D_C X_C$ and E_C in Eq. (4). When λ is larger, the reconstruction matrix $D_C X_C$ contains more intensity information, and the error matrix E_C contains less edge information. So, we can adjust the proportion of $D_C X_C$ by λ in the RSR. An appropriate value for λ is essential for visuality and its selection will be discussed in section IV.

Because l_0-minimization is an NP-hard combinatorial optimization problem, it is often relaxed to the following convex optimization problem, as suggested in [25]:

$$\min_{X_C, E_C} = \|X_C\|_1 + \lambda \|E_C\|_{2,1} \quad s.t.\ Y_C = D_C X_C + E_C \qquad (5)$$

where $||X_C||_1$ indicates the l_1-norm of the matrix X_C and is defined as.$\|X_C\|_1 = \sum_j \sum_i |X(i,j)|$. $||E_C||_{2,1}$ indicates the l_1-norm of the matrix E_C, and is defined as $\|E_C\|_{2,1} = \sum_j \sqrt{S}$. S is formulated $\sum_i E_c(i,j)^2$. i and j are coordinates of elements in the matrices X_C and E_C. Clearly, the optimization problem in Eq. (5) is convex and can be solved by some efficient tricks. In this paper, we adopt the linearized alternating direction method with the adaptive penalty (LADMAP) [26], [27] to solve the RSR decomposition.

Now that we have decomposed each channel into the reconstruction matrix and the error matrix. The component DX reflects the low frequency of each channel. It is also worth noting that we construct the dictionary D by sliding a small window on each channel of the haze image. So, RSR can describe the intensity information and edge information of the haze image very well. Based on these intrinsic properties, the component $D_L X_L$ can be approximated as fog density with depth information well, and the heavier the fog is, the greater the value of $D_L X_L$ is.

To preserve the original color information of the dehazing image, the final reconstruction matrix is obtained by weighing the reconstruction matrices of the four channels together. Thus, the ultimate haze density map is defined as follows:

$$DX = \frac{D_L X_L + D_R X_R + D_G X_G + D_B X_B}{4} \tag{6}$$

where DX is the final haze density map.

B. ESTIMATE THE TRANSMISSION MAP

Because the number of particles between the scene and the camera obviously increases with the scene depth d, the haze density map DX is positively correlated with the scene depth d. However, the medium transmission t is an exponential reduction with the scene depth d in Eq. (2). It can be inferred that the medium transmission t has a negative correlation with the haze density DX. Based on this correlation, we normalize DX from 0 to 1, and it is used to evaluate the medium transmission t of the haze image. So, $t(x)$ can be defined as follows:

$$t(x) = 1 - DX(x) \tag{7}$$

where x is the coordinates of DX matrix. The estimation of $t(x)$ in our method contains more data information and less color distortion, because $t(x)$ is constructed by using the components that are derived from four channels of the hazy image. As we can see from Fig. 5, He *et al.*'s [8] method generates the darkest results, and Kim *et al.*'s [18] results appear color distortion in the sky area. Compared with the original hazy image, the transmission map $t(x)$ estimated by our method can better reflect the state of light.

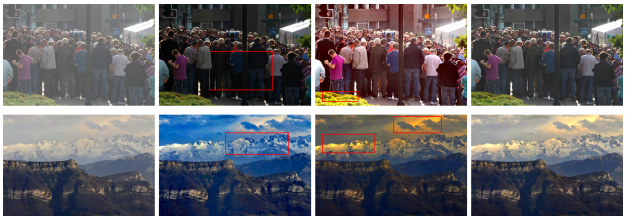

(a) (b) (c) (d)

FIGURE 5. Hazy images and dehazed images by different methods from left to right. Notice that the color distortion in the red rectangle regions. (a) Hazy images. (b) He *et al.*'s results [8]. (c) Kim *et al.*'s results [18]. (d) Our results.

In addition, we can notice that the obtained transmission map shows block artifacts on the edge areas as can be seen from Fig. 6 (b) and (c). Hence, we introduce a guided filter [28] to refine the coarser transmission map because the guided filter has the properties of a smoothed edge to eliminate block effects. The guided filter is defined by a local linear model as follows:

$$t_R(x) = a_k Y_L(x) + b_k, \quad \forall x \in \omega_k \tag{8}$$

Eq. (8) involves a guidance image and a filtering output image. In our method, the luminance map Y_L is adopted as the guidance image. It supposes that the output $t_R(x)$ is a linear transformation of Y_L in a window ω_k centered at pixel k. x is contained in all the overlapping windows ω_k. a_k and b_k are the linear coefficients, which are considered constants in ω_k. We set the rough transmission $t(x)$ as the input image I. According to [28], the coefficients of ak and bk can be calculated by the linear ridge regression model and the expressions are given as follows:

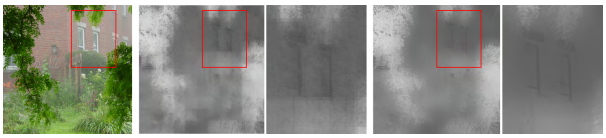

(a) (b) (c) (d) (e)

FIGURE 6. Comparison between raw transmission and refined transmission, and the enlarged edge details of the red rectangle. (a) Hazy images. (b) Raw transmission map. (c) The enlarged region of red rectangle in (b). (d) Refined transmission map by guided filter. (e) The enlarged region of red rectangle in (d).

$$a_k = \frac{\frac{1}{|\omega|}\sum_{x\in\omega_k} Y_L(x)I(x) - \mu_k \bar{I}_k}{\sigma_k^2 + \ni} \tag{9}$$

$$b_k = \bar{I}_k - a_k \mu_k \tag{10}$$

where μ_k and σ_k are the mean and variance of Y_L in the window ω_k, respectively, $|\omega|$ is the number of pixels in ω_k, $\bar{I}_k = (\sum_{x\in\omega_k} I(x))/|\omega|$ is the mean of I in ω_k, and $\in$ is a penalty term for regularization parameters in a large a_k case. Therefore, when the linear coefficients a_k and b_k are obtained, the transmission $t_R(x)$ is rewritten as follows:

$$t_R(x) = \frac{1}{|\omega|}\sum_{k|x\in\omega_k} a_k Y_L(x) + b_k \tag{11}$$

C. RECOVER THE INITIAL DEHAZED IMAGE

Because the haze density map DX is obtained from the intensity maps, it can approximate the image's local luminance. So, we estimate the atmospheric light by using the properties of DX. In the real world, the brightest pixels in the image are generally not atmospheric light [8]. Therefore, we do not select the maximum value in the hazy image as A, but to set a threshold θ to limit A. For example, if there are a few white objects such as white cars and white buildings in a hazy image, the reflected light of these white objects may cause the maximum value in DX to be greater than the threshold θ. When the intensity value of DX is greater than θ, θ is assigned to A. However, when the overall intensity of the haze image is low and all values in DX are less than θ, the maximum value in DX is assigned to A.

By extensive simulation experiments, we set 240 as the appropriate threshold θ. Compared with the previous single image dehazing methods, which regard the highest intensity pixel value as the atmospheric light A, we can obtain the more natural sky regions (see from Fig. 5).

Once the transmission $t(x)$ and the atmospheric light A are acquired, we can recover the hazy image by inverting Eq. (1)

as follows:

$$\boldsymbol{J} = \frac{\boldsymbol{I}(X) - A}{\max(t_R(x), t_0)} + A \tag{12}$$

To retain a slight fog in the dense haze area and avoid the transmission $t(x)$ equaling zero [8], the parameter t_0 is introduced to restrict the transmission to a lower bound. A typical value of t_0 is 0.1.

D. ADAPTIVE LUMINANCE TRANSFORMATION

According to the above procedure from Part 1 to Part 3 in Fig.3, a raw dehazed image is obtained. However, as can be seen, the dehazed results obtained are too bright or too dark in this way, so we need to improve the visuality of dehazed image by adjusting the brightness of the images. Inspired by [29], we design an adaptive luminance dynamic range transformation to adjust the intensity of the rough dehazed image into a more suitable range.

Based on the commonly accepted assumptions of vision behaviors, the image $J(x, y)$ can be formulated as follows [30]:

$$J(x, y) = L(x, y)R(x, y) \tag{13}$$

where $L(x, y)$ is the luminance of each pixel (x, y) and $R(x, y)$ is the reflectance. The luminance term mainly contains the mid-tone and low-frequency information, and the important visual features are included in $R(x, y)$. Therefore, the luminance and reflectance can be regarded as the base and details, respectively. According to Eq. (13), our purpose is to enhance the reflectance component $R(x, y)$ to a suitable range by compressing the dynamic range of luminance L. Therefore, in order to conduct the compression procedure on the luminance map, we transfer the dehazing image from RGB space into HSI space to extract the luminance component. The luminance component is normalized to the range [0 1] as follows:

$$L_n(x, y) = \frac{L(x, y)}{255} \tag{14}$$

The dynamic range compression can be realized by the Windowed Inverse Sigmoid (WIS) function [29], which is defined as follows:

$$f(i) = \frac{1}{1 + e^{-ai}} \tag{15}$$

The WIS function can be used to compress the dynamic range of luminance by calculating the following Eqs. (16)-(18).

$$L_n^{'} = [f(i_{\max}) - f(i_{\min})] + f(i_{\max}) \tag{16}$$

$$L_n^{''} = \ln\left(\frac{1}{L_n^{'}} - 1\right) \tag{17}$$

$$L_{enh} = \frac{L_n^{''} - i_{\min}}{i_{\max} - i_{\min}} \tag{18}$$

The normalized luminance $Ln(x,y)$ is linearly mapped from the range of [0 1] to $[f(i_{min})f(i_{max})]$ by Eq. (16). Parameters i_{min} and i_{max} are defined to change the mapping interval of

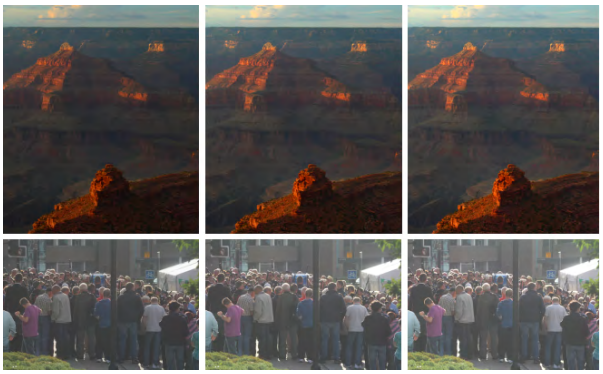

FIGURE 7. The enhanced image with different i_{min} from left to right. Left image: i_{min} is −3. Middle image: i_{min} is −4.5. right image:i_{min} is −6.

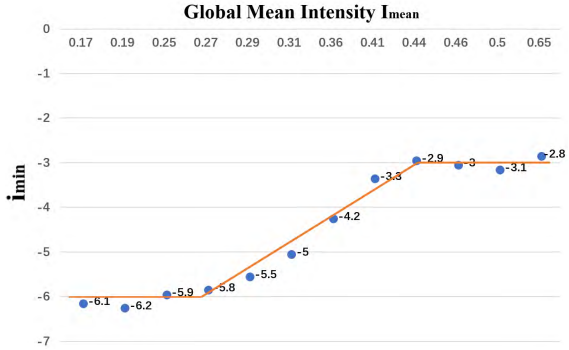

FIGURE 8. The fitted curve of function i_{min} and I_{mean}.

the normalized intensity. Eq. (17) is the inverse WIS function. The output intensity L_{enh} is normalized to [0 1] by Eq. (18).

Through the above nonlinear transfer, the final improved image L_{enh} is obtained. With this algorithm, the low-frequency components of the dehazed image are compressed, and the high frequency components of the dehazed image which contains important visual features are enhanced. According to [29], the value of i_{max} is fixed to 3, and different i_{min} yields different extents of compression and generates different results (see from Fig. 7). Obviously, for the dark dehazed image, a smaller i_{min} is more appropriate. Conversely, for the bright raw dehazed image, a larger value of i_{min} may be better. Hence, in our algorithm, an adaptive linear mapping function is designed by fitting a function of i_{min} and I_{mean} to obtain the visually refined dehazed image. As seen in Fig. 8, we first select the numbers of raw dehazed images and manually set the appropriate i_{min} to obtain the gracefully visual performance using our post-processing algorithm. Then, we compute the I_{mean} of these dehazed images. Finally, the minimum pixel value i_{min} and I_{mean} are fitted by the least square method to obtain the piecewise linear function as follows:

$$i_{\min} = \begin{cases} -6 & for\ I_{mean} < 0.27 \\ 17.6 \times I_{\min} - 10.57 & for\ 0.25 \le I_{mean} < 0.43 \\ -3 & for\ I_{mean} \ge 0.43 \end{cases} \tag{19}$$

FIGURE 9. Comparison between raw dehazed images and refined dehazed images after adaptive luminance transformation. left column: the original hazy images. Middle column: the rough dehazed images. Right column: the enhanced dehazed images.

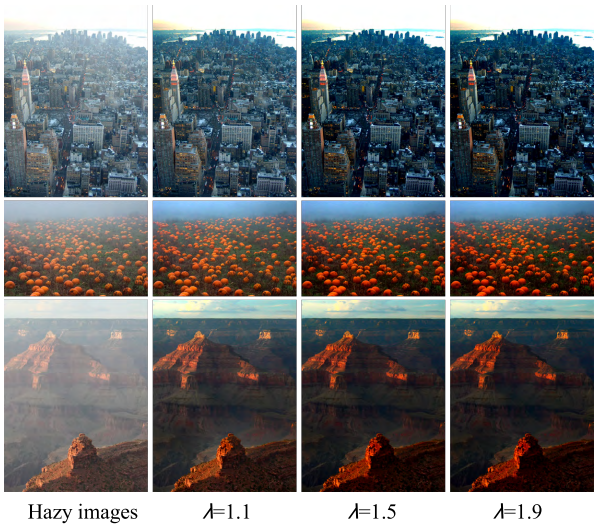

FIGURE 10. The image dehazing results with different λ. The dehazed images with small λ are bright, the dehazed images with big λ are dark.

As seen in Fig. 9, after the luminance of the dehazed images is adaptively enhanced, more details emerge.

IV. EXPERIMENT RESULTS AND ANALYSIS

In this section, the parameter settings for the experiments are firstly explained. Then, the proposed method is compared with some state-of-the-art image dehazing methods. Here, we utilize subjective comparisons and objective quality assessments to evaluate the effectiveness of the dehazing algorithms.

A. PARAMETER SELECTION

In the RSR method, different values of balance parameter λ impact the dehazing result. A larger value of λ means that more high frequency information and less luminance information are separated, which will lead to a darker dehazing result that loses many details. To get the appropriate value λ, a large number of experiments was conducted by defining different values of λ. For simplicity, three tested images, named 'city', 'pumpkin' and 'landscape' are selected to illustrate the influence of λ on the haze removal results as shown in Fig. 10. As can be seen, $\lambda = 1.1$ obtains better visual results, but the results of $\lambda = 1.5$ and $\lambda = 1.9$ are much darker. Therefore, in our experiments, λ is set to be 1.1.

B. SUBJECTIVE COMPARISON

Our experiment database includes plenty of outdoor images, thin hazy images, and heavy hazy images. Fig.11 shows the comparison of our method with the other four methods of Tarel [3], Choi *et al.* [4], He *et al.* [8], and Cai *et al.* [21] in hazy images of real scenes. In the first column, five different types of hazy images are used for comparison. As seen in the second column, Tarel's method can remove the haze by applying the filter-based method. Although the edge information and color richness are tremendously enhanced, the unnatural artifacts emerge in the examples of 'girl', 'crowd' and 'toy'. This over-enhanced inaccuracy makes the results of Tarel look very fake. Compared with Tarel's method, our method can remove the haze with faithful colors for different types of hazy images. For the third column, clear and natural dehazing results are achieved by He's method. However, the 'railway', 'crowd' and 'pumpkin' images appear to have obvious dark intensity, and this effect will lead to the disappearance of structural details. In comparison, our proposed method can improve the visual quality of the image structures and details in dark regions. Recently, deep learning method has also achieved considerable effects in image dehazing. In the fourth column, Cai's method designed an end-to-end dehazing network and obtained a comparable result. However, as we know, with the limitation of the synthetic indoor training data, it always inaccurately estimates the transmission and leads to erroneous enhancements on real-world hazy images in the heavy haze regions. For example, in 'railway' and 'crowd', the dark artifacts are obvious. Benefiting from RSR decomposition, our proposed algorithm can remove most of the haze while preserving the original color and intensity information. For the fifth column, Choi's method removes the haze by fusing the weight map over a multiscale to achieve a smooth edge. However, because this method lacks of physical information, it generates over-enhanced defog images as seen in the clothes of the 'girl' and the grass of the 'pumpkin'. However, in comparison, our physical model-based method will not be troubled by this problem.

C. OBJECTIVE QUALITY ASSESSMENT ON SYNTHETIC IMAGE

Actually, how to effectively evaluate the dehazed result has been a challenge due to lack of a ground-truth. Recently, researchers have overcome this difficulty by synthesizing haze layers on the haze-free images, which are regarded as the ground-truth. In this paper, the simulation-based

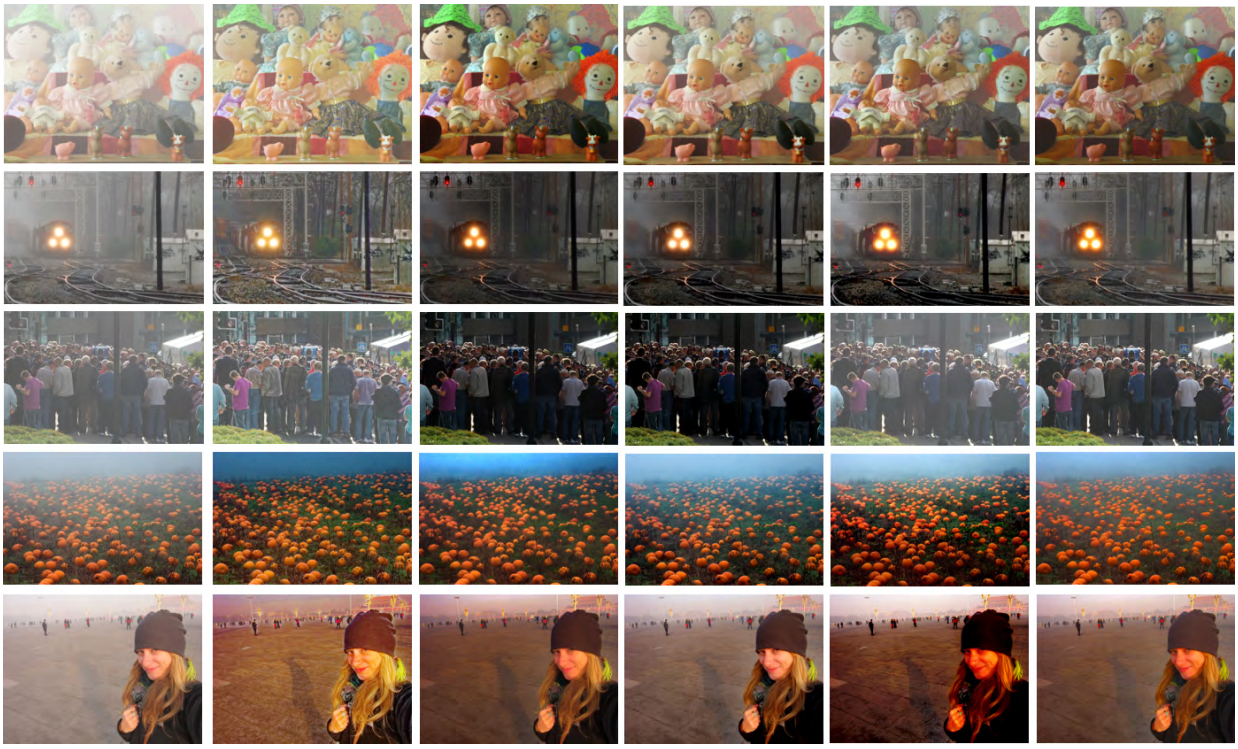

FIGURE 11. The subjective comparison experiments of real images. (a). Hazy images: they are 'toy', 'railway', 'crowd', 'pumpkin' and 'girl' from up to bottom. (b) Tarel's results. (c) He's results. (d) Cai's results. (e) Choi's results. (f) Our results.

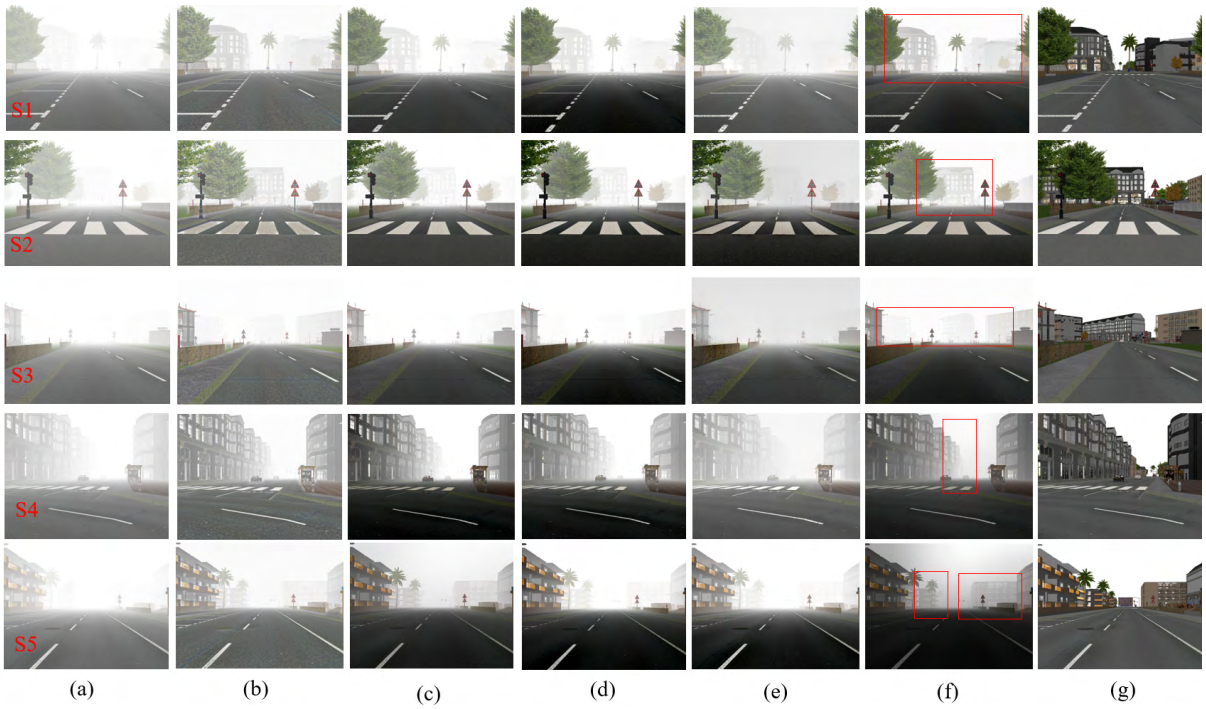

FIGURE 12. The objective comparison experiments of synthetic images. (a) Synthetic hazy images. (b) Tarel's results. (c) He's results. (d) Cai's results. (e) Choi's results. (f) Our results. (g) The ground-truth.

strategy is employed to compare the dehazed results of synthetic ground-truths to quantitatively evaluate different methods.

Referring to [5], we have compared our algorithm with Tarel's, He's, Cai's and Choi's methods using four measure indices, including *PSNRsplit*, *PSNRlum*, *Corrsplit*,

TABLE 1. Quantitative results on synthetic hazy images in terms of psnr and corr .

Hazy Images	Metrics	Tarel	He	Cai	Choi	Proposed
S1	$PSNR_{split}$	5.4052	4.5182	5.3260	5.3078	**5.7033**
S2		5.6502	5.6096	5.5042	5.8074	**6.0136**
S3		5.5763	5.5825	5.5231	5.7001	**5.9844**
S3		5.4658	5.6241	5.4424	5.0667	**6.1411**
S5		5.7330	5.6064	5.5509	5.7676	**6.0962**
S1	$PSNR_{lum}$	11.1624	8.2704	10.848	10.795	**12.225**
S2		12.0223	11.872	11.481	12.621	**13.431**
S3		11.8651	11.878	11.638	12.299	**13.435**
S4		11.3077	11.889	11.219	9.8982	**13.923**
S5		12.3857	11.883	11.680	12.509	**13.813**
S1	$CORR_{split}$	1.3471	1.1031	1.2930	1.2746	**1.3597**
S2		1.4080	1.3714	1.3685	1.3459	**1.4509**
S3		1.3561	1.3215	1.3155	1.2855	**1.3677**
S4		1.2727	1.2599	1.2134	1.1503	**13.923**
S5		1.3941	1.3830	1.3541	1.3162	**1.4420**
S1	$CORR_{lum}$	0.6479	0.3656	0.5896	0.5653	**0.6556**
S2		0.7109	0.6760	0.6733	0.6461	**0.7542**
S3		0.6643	0.6312	0.6250	0.5893	**0.6780**
S4		0.5647	0.5469	0.4921	0.4057	**0.6260**
S5		0.7130	0.7007	0.6736	0.6331	**0.7565**

Corrlum, which are defined based on the peak-signal-to-noise ratio (*PSNR*) and correlation (*Corr*). The *PSNRsplit* index is obtained by combining *PSNRs* of each channel of the image using the *l2* -norm. The expression is as follows:

$$PSNR_{spilt} = \sqrt{\sum_{c=r,g,b} \left\| PSNR(I_c^{GT}, I_c^r) \right\|_2} \tag{20}$$

where I_c^{GT} is the ground-truth image, and I_c^r is the dehazed image result. c is the color channels. The $PSNR_{lum}$ is the *PSNR* of the luminance of the image. It is defined as follows:

$$PSNR_{lum} = PSNR(I_{lum}^{GT}, I_{lum}^r) \tag{21}$$

where I_{lum}^{GT} is the luminance map of the ground-truth, and Ilumr is the luminance map of the dehazed image. Likewise, the two correlation-based measures $Corr_{split}$ and $Corr_{lum}$ are defined as follows:

$$Corr_{spilt} = \sqrt{\sum_{c=r,g,b} \left\| Corr(I_c^{GT}, I_c^r) \right\|_2} \tag{22}$$

$$Corr_{lum} = Corr(I_{lum}^{GT}, I_{lum}^r) \tag{23}$$

$Corrs_{split}$ is the correlation coefficient of the color channel between the dehazed image and the ground-truth, and $Corr_{lum}$ is the correlation coefficient of the luminance map between the dehazed image and the ground-truth.

The *PSNR* is introduced to measure the degree of similarity between the dehazed image and the haze-free ground-truth, and *Corr* is used to measure the correlation between the dehazed image and the haze-free ground-truth. For each of the evaluation measure indices, a higher value indicates that the dehazing image is more similar to the corresponding haze-free ground-truth and that the dehazing method is more effective. Here, we take a large number of experiments on the commonly used synthetic stereo FRIDA database [31], in which five synthetic haze-free and the corresponding hazy stereo images are shown and named as S1 to S5. Fig.12 shows the dehazing results of Tarel's, He's, Choi's, Cai's and our method. In comparison, our method can recover more structural information and outperforms the other four methods in visual effect. The other methods have difficulties in handling the heavy haze. For example, the dense dehaze in the distance marked with red rectangle in Fig.12 cannot sufficiently be removed by the other methods. Furthermore, from the dehazing results, we can also see that the objects in the distance are surrounded by dense fog and the color tone of the images is over-bright. In contrast, our method obtains clearer dehazing results such as the house and tree hidden in the heavy haze.

TABLE 1 gives the quantitative results of different methods. As seen from TABLE 1, our proposed results produce the highest measure values for all test images, which demonstrate that our dehazed results are more similar to the haze-free ground-truth images. Therefore, from all above analysis, we can conclude that the proposed method

outperforms other methods in both the objective and subjective evaluations, and produces better dehazing results with more details and less color distortions.

V. CONCLUSION

In this paper, we have proposed an efficient single image haze removal method based on RSR. We first construct the dictionary from the four channels to extract the intensity maps of the degraded hazy image. Then, to reduce the color distortions, the haze density map is obtained by weighting the intensity maps to effectively estimate the transmission map. Finally, the dehazing results can be obtained by solving the atmospheric scattering model. Furthermore, an adaptive luminance transformation is defined to adjust the visual effect of the dehazing image. In this way, the proposed method can alleviate the distortion caused by the loss of original information and make the output dehazing image look more natural. The experiments prove that our method achieves relatively better results on denser haze images and outperforms the state-of-the-art techniques. Since it is necessary to learn an effective dictionary in our proposed method, which is based on RSR decomposition, our method is not the fastest among all methods. It will be further optimized in the future by learning an independent dictionary before performing the fog removal operation.

REFERENCES

[1] Y. Xu, J. Wen, L. Fei, and Z. Zhang, "Review of video and image defogging algorithms and related studies on image restoration and enhancement," *IEEE Access*, vol. 4, pp. 165–188, 2016.
[2] R. T. Tan, "Visibility in bad weather from a single image," in *Proc. IEEE Conf. Comput. Vis. Pattern Recognit. (CVPR)*, Jun. 2008, pp. 1–8.
[3] J.-P. Tarel and N. Hautière, "Fast visibility restoration from a single color or gray level image," in *Proc. IEEE Int. Conf. Comput. Vis.*, Sep./Oct. 2009, pp. 2201–2208.
[4] L. K. Choi, J. You, and A. C. Bovik, "Referenceless prediction of perceptual fog density and perceptual image defogging," *IEEE Trans. Image Process.*, vol. 24, no. 11, pp. 3888–3901, Nov. 2015.
[5] A. Galdran, J. Vazquez-Corral, D. Pardo, and M. Bertalmío, "Fusion-based variational image dehazing," *IEEE Signal Process. Lett.*, vol. 24, no. 2, pp. 151–155, Feb. 2017.
[6] P. S. Chavez, Jr., "An improved dark-object subtraction technique for atmospheric scattering correction of multispectral data," *Remote Sens. Environ.*, vol. 24, no. 3, pp. 459–479, Apr. 1988.
[7] R. Fattal, "Single image dehazing," *ACM Trans. Graph.*, vol. 27, no. 3, p. 72, Aug. 2008.
[8] K. He, J. Sun, and X. Tang, "Single image haze removal using dark channel prior," *IEEE Trans. Pattern Anal. Mach. Intell.*, vol. 33, no. 12, pp. 2341–2353, Dec. 2011.
[9] D. Park, D. K. Han, and H. Ko, "Single image haze removal with WLS-based edge-preserving smoothing filter," in *Proc. IEEE Int. Conf. Acoust., Speech Signal Process.*, May 2013, pp. 2469–2473.
[10] J. Yu, C. Xiao, and D. Li, "Physics-based fast single image fog removal," in *Proc. IEEE Int. Conf. Signal Process.*, Oct. 2010, pp. 1048–1052.
[11] K. B. Gibson and T. Q. Nguyen, "Fast single image fog removal using the adaptive Wiener filter," in *Proc. Int. Conf. Image Process.*, Sep. 2013, pp. 714–718.
[12] S.-C. Huang, B.-H. Chen, and W.-J. Wang, "Visibility restoration of single hazy images captured in real-world weather conditions," *IEEE Trans. Circuits Syst. Video Technol.*, vol. 24, no. 10, pp. 1814–1824, Oct. 2014.
[13] S.-C. Huang, J.-H. Ye, and B.-H. Chen, "An advanced single-image visibility restoration algorithm for real-world hazy scenes," *IEEE Trans. Ind. Electron.*, vol. 62, no. 5, pp. 2962–2972, May 2015.
[14] G. Meng, Y. Wang, J. Duan, S. Xiang, and C. Pan, "Efficient image dehazing with boundary constraint and contextual regularization," in *Proc. IEEE Int. Conf. Comput. Vis. (ICCV)*, Dec. 2013, pp. 617–624.
[15] K. Nishino, L. Kratz, and S. Lombardi, "Bayesian defogging," *Int. J. Comput. Vis.*, vol. 98, no. 3, pp. 263–278, Jul. 2012.
[16] Y. Wang and C. Fan, "Single image defogging by multiscale depth fusion," *IEEE Trans. Image Process.*, vol. 23, no. 11, pp. 4826–4837, Nov. 2014.
[17] N. Hautiére, J.-P. Tarel, and D. Aubert, "Towards fog-free in-vehicle vision systems through contrast restoration," in *Proc. IEEE Conf. Comput. Vis. Pattern Recognit.*, Jun. 2007, pp. 1–8.
[18] J.-H. Kim, W.-D. Jang, J.-Y. Sim, and C.-S. Kim, "Optimized contrast enhancement for real-time image and video dehazing," *J. Vis. Commun. Image Represent.*, vol. 24, no. 3, pp. 410–425, Apr. 2013.
[19] K. Tang, J. Yang, and J. Wang, "Investigating haze-relevant features in a learning framework for image dehazing," in *Proc. IEEE Conf. Comput. Vis. Pattern Recognit.*, Jun. 2014, pp. 2995–3000.
[20] Q. Zhu, J. Mai, and L. Shao, "A fast single image haze removal algorithm using color attenuation prior," *IEEE Trans. Image Process.*, vol. 24, no. 11, pp. 3522–3533, Nov. 2015.
[21] B. Cai, X. Xu, K. Jia, C. Qing, and D. Tao, "DehazeNet: An end-to-end system for single image haze removal," *IEEE Trans. Image Process.*, vol. 25, no. 11, pp. 5187–5198, Nov. 2016.
[22] C. Li, J. Guo, F. Porikli, H. Fu, and Y. Pang, "A cascaded convolutional neural network for single image dehazing," *IEEE Access*, vol. 6, pp. 24877–24887, 2018.
[23] Q. Zhang and M. D. Levine, "Robust multi-focus image fusion using multi-task sparse representation and spatial context," *IEEE Trans. Image Process.*, vol. 25, no. 5, pp. 2045–2058, May 2016.
[24] J. Wright, A. Y. Yang, A. Ganesh, S. S. Sastry, and Y. Ma, "Robust face recognition via sparse representation," *IEEE Trans. Pattern Anal. Mach. Intell.*, vol. 31, no. 2, pp. 210–227, Feb. 2009.
[25] G. Liu, Z. Lin, S. Yan, J. Sun, Y. Yu, and Y. Ma, "Robust recovery of subspace structures by low-rank representation," *IEEE Trans. Pattern Anal. Mach. Intell.*, vol. 35, no. 1, pp. 171–184, Jan. 2013.
[26] Z. Lin, R. Liu, and Z. Su, "Linearized alternating direction method with adaptive penalty for low-rank representation," in *Proc. Adv. Neural Inf. Process. Syst.*, 2011, pp. 1–9.
[27] Y. Zhang, Z. Jiang, and L. S. Davis, "Learning structured low-rank representations for image classification," in *Proc. IEEE Conf. Comput. Vis. Pattern Recognit.*, Jun. 2013, pp. 676–683.
[28] K. He, J. Sun, and X. Tang, "Guided image filtering," *IEEE Trans. Pattern Anal. Mach. Intell.*, vol. 35, no. 6, pp. 1397–1409, Jun. 2013.
[29] L. Tao, R. C. Tompkins, and V. K. Asari, "An illuminance-reflectance model for nonlinear enhancement of color images," in *Proc. IEEE Conf. Comput. Vis. Pattern Recognit.*, Sep. 2005, p. 159.
[30] B. K. P. Horn, "Determining lightness from an image," *Comput. Graph. Image Process.*, vol. 3, no. 4, pp. 277–299, 1974.
[31] J. P. Tarel, N. Hautière, A. Cord, D. Gruyer, and H. Halmaoui, "Improved visibility of road scene images under heterogeneous fog," in *Proc. IEEE Intell. Veh. Symp.*, Jun. 2010, pp. 478–485.

SHUYING HUANG (M'14) received the Ph.D. degree in computer application technology from the Ocean University of China, Qingdao, China, in 2013. She is currently an Associate Professor with the School of Software and Communication Engineering, Jiangxi University of Finance and Economics, Nanchang, China. Her current research interests include image and signal processing, and pattern recognition.

DONGLEI WU received the B.S. degree in electronic and information engineering from the Chengdu College, University of Electronic Science and Technology of China, Chengdu, China, in 2015. He is currently pursuing the M.S. degree in electronics and communication engineering with the Jiangxi University of Finance and Economics, Nanchang, China. His current research interests include image dehazing, image processing, computer vision, and deep learning.

YONG YANG (M'13–SM'16) received the Ph.D. degree from Xi'an Jiaotong University, Xi'an, China, in 2005. From 2009 to 2010, he was a Post-Doctoral Research Fellow with Chonbuk National University, Jeonju, South Korea. He is currently a Full Professor and the Vice Dean with the School of Information Technology, Jiangxi University of Finance and Economics, Nanchang, China. His current research interests include image fusion, image super-resolution reconstruction, medical image processing and analysis, and pattern recognition. He is an Associate Editor of the IEEE Access and an Editor of the *KSII Transactions on Internet and Information Systems*. He received the title of the Jiangxi Province Young Scientist in 2012. He was selected as the Jiangxi Province Thousand and Ten Thousand Talent in 2015.

HAIJUN ZHU received the B.S. degree in hydrology and water resources engineering from the East China University of Technology, Nanchang, China, in 2016. He is currently pursuing the M.S. degree in electronic and communication engineering with the Jiangxi University of Finance and Economics, Nanchang. His current research interests include image superresolution, deep learning, and image classification.